Experimental observation of fractional echoes

G. Karras, E. Hertz, F. Billard, B. Lavorel, G. Siour, J. -M. Hartmann, O. Faucher, Erez Gershnabel, Yehiam Prior, Ilya Sh. Averbukh

Experimental observation of fractional echoes

G. Karras,[1] E. Hertz,[1] F. Billard,[1] B. Lavorel,[1] G. Siour,[2] J.-M. Hartmann,[2] O. Faucher,[1,*] Erez Gershnabel,[3] Yehiam Prior,[3] and Ilya Sh. Averbukh[3,†]

[1]*Laboratoire Interdisciplinaire CARNOT de Bourgogne, UMR 6303 CNRS-Université Bourgogne Franche-Comté, BP 47870, 21078 Dijon, France*

[2]*Laboratoire Interuniversitaire des Systèmes Atmosphériques (LISA) CNRS (UMR 7583), Université Paris Est Créteil, Université Paris Diderot, Institut Pierre-Simon Laplace, Université Paris Est Créteil, 94010 Créteil Cedex, France*

[3]*AMOS and Department of Chemical Physics, Weizmann Institute of Science, Rehovot 76100, Israel*

(Received 16 March 2016; revised manuscript received 18 May 2016; published 6 September 2016)

We report the observation of fractional echoes in a double-pulse excited nonlinear system. Unlike standard echoes, which appear periodically at delays which are integer multiples of the delay between the two exciting pulses, the fractional echoes appear at rational fractions of this delay. We discuss the mechanism leading to this phenomenon, and provide experimental demonstration of fractional echoes by measuring third harmonic generation in a thermal gas of CO_2 molecules excited by a pair of femtosecond laser pulses.

DOI: 10.1103/PhysRevA.94.033404

Many nonlinear systems display the phenomenon of echoes, which is a series of delayed impulsive responses after a pair of short external pulses. These echoes typically show themselves at times $\tau \sim T, 2T, 3T$, etc., after the end of the excitation, where T is the delay between the stimulating pulses. Echoes are common in many areas of physics, including NMR [1], plasma physics [2–4], nonlinear optics [5], cavity quantum electrodynamics [6,7], and cold-atom physics [8–11]. Echoes were predicted to occur in proton storage rings [12,13] and were observed in high-energy hadron beam experiments [14,15]. Echo-enabled generation of short-wavelength radiation in free-electron lasers [16–18] was demonstrated (for a recent review, see Ref. [19]).

Recently we reported the existence of orientation and alignment echoes in an ensemble of free classical rotors stimulated by two successive impulsive forces [20]. We attributed the echo formation to the kick-induced filamentation of the rotational phase space, and demonstrated the effect experimentally in a gas of CO_2 molecules excited by a pair of femtosecond laser pulses. The time-dependent mean molecular alignment (defined as $\langle \cos^2(\theta) \rangle(t)$, where θ is the angle between the molecular axis and laser polarization) was measured via the laser-induced birefringence signal. The excited system exhibited a regular sequence of echo pulses at delays $\tau = T, 2T, 3T, \ldots$. In addition, our theoretical analysis and numerical simulations [20] also predicted additional remarkable recurrences (fractional echoes) at $\tau = (p/q)T$, where p and q are mutually prime numbers. These fractional echoes, however, cannot be seen in the alignment signal since they require measurement of higher order moments of the molecular angular distribution.

Here we present our observation of the phenomenon of fractional echoes measured via third-harmonic generation (THG) in a gas of CO_2 molecules at room temperature. In what follows we introduce the mechanism of the fractional echoes by using a simple two-dimensional (2D) classical model, and then describe our experiments in which this phenomenon was observed. We also compare the experimental results to full three-dimensional (3D) classical and quantum simulations of the echo formation.

For a nonresonant laser field interacting with a symmetric linear molecule, such as N_2, O_2, or CO_2, the angular-dependent interaction potential is $V(\theta,t) = -(\Delta\alpha/4)E^2(t)\cos^2(\theta)$ [21,22]. Here $\Delta\alpha$ is the polarizability anisotropy, and $E(t)$ is the envelope of the laser pulse. As is well known, such an interaction leads to the alignment of the molecular axis along the field polarization direction (for reviews on molecular alignment, see Refs. [23–27]). Consider a 2D ensemble of rotors that are initially uniformly dispersed in angle θ, and have a spread in angular velocity ω with a Gaussian distribution. The phase space probability distribution at time t after the first linearly polarized short laser pulse (δ kick) is given by [20]

$$f(\omega,\theta,t) = \frac{1}{2\pi}\frac{1}{\sqrt{2\pi}\sigma}\exp\left\{-\frac{[\omega - \Omega\sin(2\omega t - 2\theta)]^2}{2\sigma^2}\right\}. \quad (1)$$

Here Ω is proportional to the time-integrated intensity (total energy) of the pulse. Note that Eq. (1) is written specifically for the polarization-type interaction. Shortly after the kick, the shape of the density distribution folds [Fig. 1(a)], resulting in transient alignment along the direction $\theta = 0$. On a longer time scale, the probability density of Eq. (1) develops multiple parallel filaments separated in angular velocity by π/t, where t is the evolution time [Fig. 1(b)]. The number of these filaments grows with time, and their width is diminishing. Filamentation of the phase space is a phenomenon well known in statistical mechanics of stellar systems [28] and in accelerator physics [29]. Moreover, the transient alignment caused by folding of the phase space [see Fig. 1(a)] has much in common with the bunching effect observed in particle accelerators. Following the second kick at $t = T$, every filament in Fig. 1(b) forms a folded pattern like in Fig. 1(a). Because of the frequency shift π/T between the neighboring filaments, most of the time τ after the second pulse these folded features are displaced with respect to each other, which results in a quasiuniform total angular distribution considered as a function of θ only. As previously discussed [20], at time

*olivier.faucher@u-bourgogne.fr
†ilya.averbukh@weizmann.ac.il

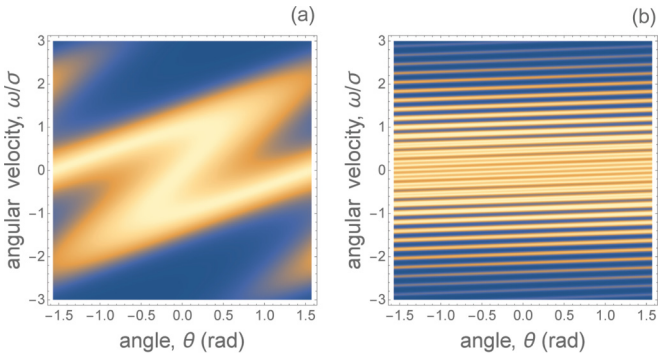

FIG. 1. Filamentation of the phase space density distribution. $\Omega/\sigma = 1$, (a) $\sigma t = 1$, (b) $\sigma t = 15$.

$\tau \sim T$, the folds in the filaments bunch up near $\theta = 0$ due to the "quantization" of the angular velocity of the strips, resulting in an echo in the alignment factor $\langle\cos^2(\theta)\rangle$, with higher order echoes at delays $2T, 3T, \ldots$, after the second pulse. An analytic expression for the time-dependent alignment signal is given in Eq. (S-5) in the Supplemental Material of Ref. [20], and it fully supports these general geometric arguments.

Here, however, we are interested in the highly symmetric structures in the phase space, which appear at $\tau = T/2, T/3, \ldots$, when synchronization and bunching of the folded features from non-neighboring filaments happens (see Fig. 2 as an example). As discussed in Ref. [20], these patterns may be associated with the so-called fractional echoes. These echoes are not seen in a mere alignment signal $\langle\cos^2(\theta)\rangle$, but require measuring higher order observables $\langle\cos(2n\theta)\rangle$ $(n > 1)$. The simple 2D model considered here allows for obtaining an analytical expression for the time-dependent mean value of $\langle\cos(2n\theta)\rangle$:

$$\langle\cos(2n\theta)\rangle(\tau) = \sum_{k=0}^{k=\infty} (-1)^k e^{-2\sigma^2(n\tau - kT)^2} J_{k+n} \times [2n\Omega_2\tau] J_k[2n\Omega_1(n\tau - kT)], \quad (2)$$

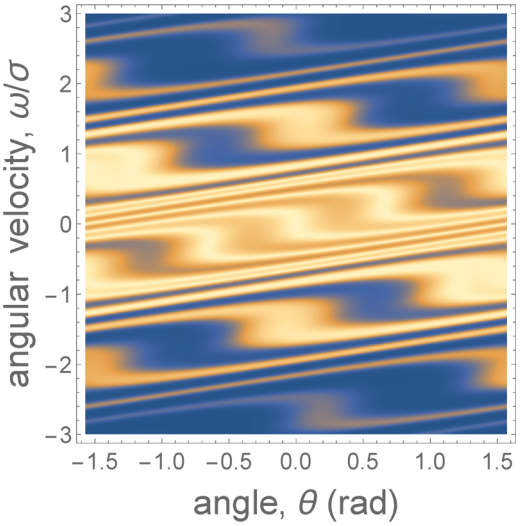

FIG. 2. Fractional echo in the filamented phase space. $\Omega_1/\sigma = 1$, $\sigma T = 5$, $\Omega_2/\Omega_1 = 1/3$, and $\sigma\tau = 2.293$; fractional echo near $\tau \approx T/2$ is formed.

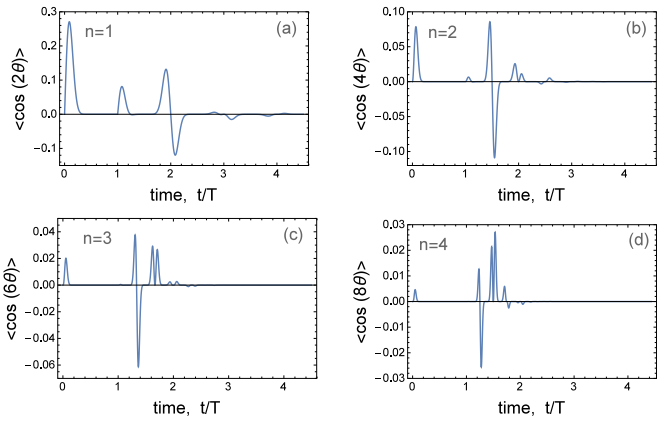

FIG. 3. Mean values $\langle\cos(2n\theta)\rangle$ vs time after the first kick. $\Omega_1/\sigma = 1$, $\sigma T = 5$, $\Omega_2/\Omega_1 = 1/3$. (a) $n = 1$, (b) $n = 2$, (c) $n = 3$, (c) $n = 4$.

where $J_m(z)$ is the mth order Bessel function of the first kind. Equation (2) presents a sequence of signals localized in time near $\tau = \frac{k}{n}T$ where k is an integer. For $n > 1$, these are the above-mentioned fractional echoes, while $n = 1$ corresponds to the regular alignment echoes. Figure 3 presents the calculated mean values $\langle\cos(2n\theta)\rangle$ versus time after the first kick. It is clearly seen that the initial transient response shortly after the second pulse is followed by a series of fractional echoes at $\tau \sim T/2, T/3$, etc.

All these findings derived in the simplified 2D classical model are confirmed by the results of the fully 3D simulations (both classical and quantum mechanical) presented below in Figs. 4(b), 6(b), and 7(b). For details of our 3D computational procedures, see Ref. [25] and references there as well as Ref. [30]. Movie M1 in the Supplemental Material [31] shows the simulated evolution of the angular distribution of an ensemble of 3D classical rotors kicked by two delayed pulses. In addition to common alignment events observed just after the pulses and near times of full echoes, high-order transient symmetric structures can be seen in the angular distribution, which correspond to the fractional echoes (compare with Fig. 2).

Next, we describe our experiments, where fractional echoes were observed by third harmonic generation in a thermal gas of CO_2 molecules excited by a pair of femtosecond laser pulses. In our previous work [20], the observation of the rotational alignment echoes in laser-kicked molecules was performed by using a time-resolved birefringence technique providing a signal $\mathcal{S}_{\text{bir.}}$ sensitive to $\langle\cos^2(\theta)\rangle$

$$\mathcal{S}_{\text{bir.}}(\tau) \propto \int_{-\infty}^{\infty} I_{\text{pr}}(\tau' - \tau)\left[\langle\cos^2(\theta)\rangle(\tau') - \frac{1}{3}\right]^2 d\tau', \quad (3)$$

with I_{pr} the intensity of the probe pulse. Figure 4(a) presents the birefringence signal recorded in CO_2 molecules by employing the experimental setup detailed in Ref. [20]. Measurements were performed at room temperature for a pressure of 80 mbar. As indicated in the figure legend, the first pump pulse $\mathcal{P}1$ (intensity $I_1 \approx 50$ TW/cm^2), the second pump pulse $\mathcal{P}2$ (intensity $I_2 \approx 10$ TW/cm^2), and the echoes are colored in red, blue, and yellow, respectively. The first echo appears around $\tau = T = 2.5$ ps, where T is the relative delay between $\mathcal{P}1$

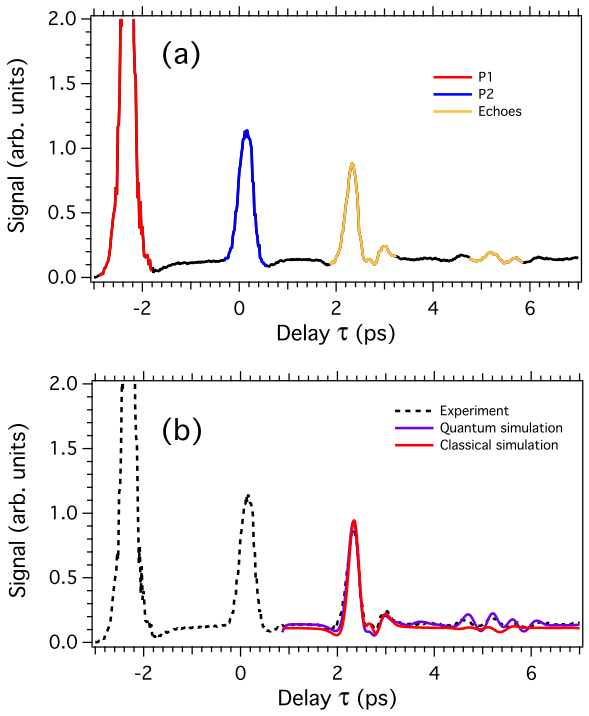

FIG. 4. (a) Birefringence signal as a function of the delay τ between $\mathcal{P}2$ and the probe pulse. Only the range corresponding to the quarter rotational period of the CO_2 (i.e., $T + \tau < T_{\rm rev}/4 = 10.67$ ps) is shown. The delay T between $\mathcal{P}1$ and $\mathcal{P}2$ is set to 2.5 ps. (b) Comparison between the experiment (dotted black line) and quantum (solid purple line) and classical (solid red line) simulations (see text).

and $\mathcal{P}2$. The second echo (i.e., higher order echo) is detected around $\tau = 2T = 5$ ps, as expected from the above classical arguments. Figure 4(b) compares the measured signal with the results of the 3D simulations of the birefringence signal, both classical (red curve) and fully quantum mechanical (purple curve). As seen, the classical treatment nicely describes the shape of the first echo, in agreement with the classical origin of this phenomenon. However, the shape of the second echo is already affected by the quantum effects that become important as the delay time $t = T + \tau$ approaches $T_{\rm rev}/4$ —a quarter of the rotational revival period. The intensity dependence of the echo signal with respect to $\mathcal{P}1$ and $\mathcal{P}2$ has been studied in Ref. [20]. The signal observed in Fig. 4(a) results from the orientational contribution to the optical Kerr effect [32] and therefore only provides information about the observable $\langle\cos^2(\theta)\rangle$. This is the reason why fractional echoes cannot be observed with this technique. In order to reveal fractional echoes, the system must be probed through a higher-order nonlinear process sensitive to $\langle\cos^{2m}(\theta)\rangle$, with the integer $m > 1$. Harmonic generation can serve this goal. It has been shown theoretically [33–37] and experimentally [38,39] that high-order harmonic spectra generated from aligned molecules carry information about higher-order cosine moments. The time dependence of the harmonic amplitude can be generally described by a series of direction cosine products governing the dynamical alignment. The trigonometric terms involved in this expression depend on the molecular system and the harmonic order. For instance, the time dependence of the third-harmonic generation in aligned CO_2 is governed by a combination of observables $\langle\cos^2(\theta)\rangle$ and $\langle\cos^4(\theta)\rangle$ [40].

In a recent publication [41], it was shown that a sensitive background-free detection of dynamical alignment could be achieved by generating the THG from a circularly polarized field. As a result of the axial symmetry introduced by the anisotropic alignment, the THG field driven by a circularly polarized pump is elliptically polarized. The helicity of the harmonic field is governed by the time delay between the alignment pulse and the driving field. This effect is used in the present work in order to observe the fractional echoes in CO_2. The signal recorded along each polarization component of the THG field is described in the framework of perturbation theory by the following expression [42,43]:

$$\mathcal{S}_{i_{\rm THG}}(\tau) \propto \int_{-\infty}^{\infty} I_{\rm pr}^3(\tau' - \tau)\Big[\alpha_i\Big(\langle\cos^2(\theta)\rangle(\tau') - \frac{1}{3}\Big) + \beta_i\Big(\langle\cos^4(\theta)\rangle(\tau') - \frac{1}{5}\Big)\Big]^2 d\tau', \quad (4)$$

where $i = y,z$ are the polarization components of the THG field, with z being the direction of alignment of the molecule, and α_i, β_i are two parameters that depend on the second-order hyperpolarizability components of the molecule [41]. In order to highlight the presence of the fractional echo, the measurements are conducted by selecting one of the two THG field components [41].

The experimental setup for producing THG in aligned molecules is depicted in Fig. 5. The pump and probe IR pulses are produced by a 1 kHz amplified Ti:sapphire laser operating at 800 nm. The pump beam is divided into two pulses denoted as $\mathcal{P}1$ and $\mathcal{P}2$, respectively. The relative delays between the three pulses are controlled by two motorized stages. They allow achieving an accurate adjustment of the delay T between $\mathcal{P}1$ and $\mathcal{P}2$, and τ between $\mathcal{P}2$ and the probe pulse, respectively. The energy of each pulse is adjusted by combining a half wave-plate with a Glan polarizer. The pump pulses $\mathcal{P}1$ and $\mathcal{P}2$ are linearly polarized, while the polarization

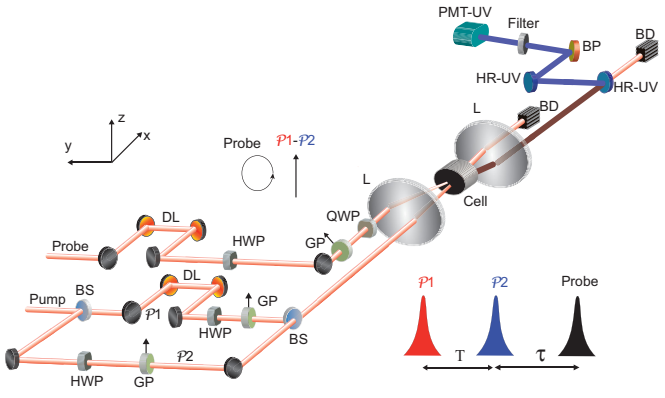

FIG. 5. Experimental setup. A, analyzer; BS, beam splitter; GP, Glan polarizer; HWP, zero-order half wave-plate; QWP, zero-order quarter wave-plate; PMT, photo multiplier tube; L, lens; DL, delay line; BD, beam dumper; HR-UV, high-reflectivity dielectric UV mirror; and BP, silica plate set at Brewster's angle. The polarizations of the different pulses along with a relative timing chart are shown in the insets.

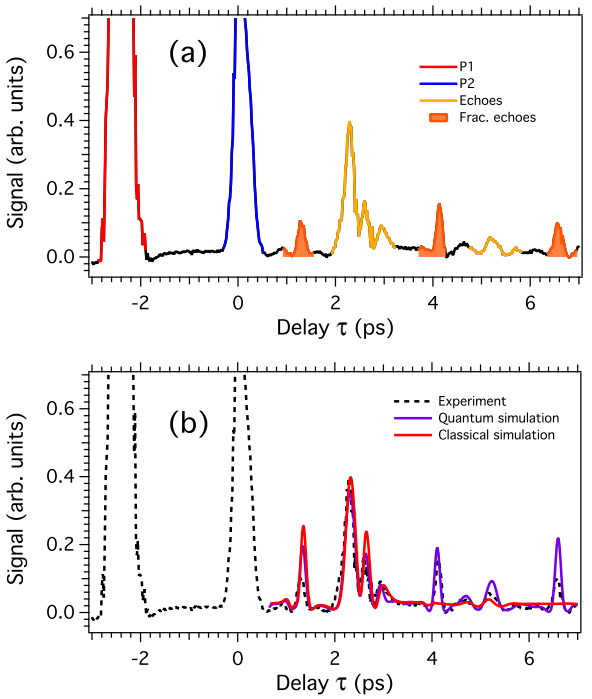

FIG. 6. (a) Third-harmonic (THG) signal detected by selecting the harmonic field component parallel to the alignment axis z. The delay T between $\mathcal{P}1$ and $\mathcal{P}2$ is set to 2.5 ps. (b) Comparison between the experiment (dotted black line) and quantum (solid purple line) and classical (solid red line) simulations.

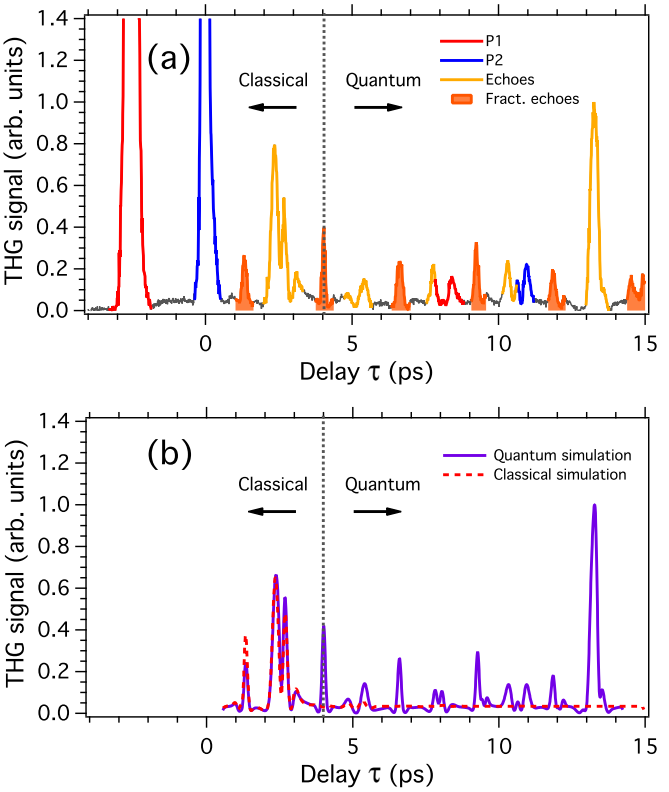

FIG. 7. (a) Signal detected along the vertical z component of the THG field. The delay T between $\mathcal{P}1$ and $\mathcal{P}2$ is set to 2.6 ps. $I_1 \approx 45$ TW/cm^2, $I_2 \approx 11$ TW/cm^2. (b) Theoretically simulated THG signals: quantum (solid purple line) and classical (dotted red line) simulations.

of the probe is set circular. The three beams are crossed with a small angle ($\sim 4^\circ$) and focused with a lens ($f = 15$ cm) inside a static cell filled with CO_2 molecules at room temperature and at the same pressure (80 mbar) as in Fig. 4. After the cell and a collimating lens, the two pump beams are guided to a beam dumper. The third harmonic generated by the probe is reflected by two high reflectivity mirrors at 266 nm and a band-pass filter for the removal of the fundamental IR frequency component. The polarization-sensitive detection is achieved by using a fused silica plate set at Brewster's angle. Finally, the THG signal is recorded using a photomultiplier tube.

The THG signal detected along the polarization direction of the pump field is shown in Fig. 6(a). The parameters of the pump pulses $\mathcal{P}1$ and $\mathcal{P}2$ are similar to the ones used for the birefringence measurement of Fig. 4(a). The energy of the probe is similar to $\mathcal{P}1$. The echo and high-order echoes are observed with the same timing as in the birefringence measurement. However, their structural shapes differ due to the contribution of the observable $\langle \cos^4(\theta) \rangle$ to the THG signal. The main difference between Figs. 4(a) and 6(a) is the presence of the fractional echoes in the THG signal (colored in orange) around $\tau = T/2 = 1.25$ ps together with the occurrence of the higher orders around $\tau = 3T/2 = 3.75$ ps and $\tau = 5T/2 = 6.25$ ps, respectively. Figure 6(b) compares experimental signals with the results of our classical and quantum simulations of the THG process. As in the case of the birefringence measurements, the classical and quantum results are practically indistinguishable in the region of the first full echo at $\tau = T = 2.5$ ps, and agree reasonably well near the first fractional echo at $\tau = T/2 = 1.25$ ps. Moreover, both curves are in good agreement with the experimental data. However, the classical treatment fails to catch a signal peak near $\tau = 4$ ps, while the quantum modeling reproduces it precisely. Figure 7(a) shows the THG signal recorded up to 15 ps, i.e., reaching the region near $t \sim T_{\text{rev}}/2$ where the quantum nature of the rotational motion is obviously important. Figure 7(b) compares it with the results of the fully quantum 3D simulation of the THG process, which are in excellent agreement with our measurements. For evolution times shorter than ~ 4 psec, the agreement with the 3D classical calculation is also good enough. Multiple spikes in the THG signal seen on the longer time scale result from the interplay between the classical echo effect and the quantum revival phenomenon.

In conclusion, we observed fractional echoes in the third-harmonic signal arising from a thermal gas of CO_2 molecules following excitation by a pair of femtosecond laser pulses. These transient responses of the system occur at times which are rational fractions of the delay between the two kicking pulses. We compared the experimental observations to both quantum and classical simulations. Quantum mechanics, of course, and as is shown by our simulations, explains the observed interaction between the exciting pulses and the molecules. The phenomenon of fractional echoes, however, is well described by classical analysis on short time scales, and is actually a classical effect. In the present case, since we study the fractional echoes in a molecular system where quantum revivals are also present, a word of caution is needed.

While echoes and revivals both show recurrences of an original impulse excitation, these are distinctly different phenomena which cannot be derived one from the other. The appearance of revivals, full or fractional [44,45], is a quantum effect which does not exist in classical systems. Revivals are observed after a single-pulse excitation, and their period is determined by the properties of the rotational energy spectrum. Echoes, on the other hand, appear only after two pulses and are common to many physical systems, including macroscopic ones, where classical mechanics is naturally applicable, as well as molecular systems; their timing is determined by the fully controlled delay between the two exciting pulses. On longer time scales, the interplay between the echoes and the quantum revivals shows up both in our experiments and in the numerical simulations.

The fractional molecular echoes described here may be beneficial for very short-time pump-probe measurements in molecular gases by providing new tools for better insight into dissipative and decoherence processes. Similar to the revival structures, fractional echoes may shed light on the features of high-order harmonic generation in molecules. The discussed classical mechanism leading to fractional echoes is rather general, and these same echoes should be observable in related systems such as, e.g., the betatron oscillations of a beam in hadron accelerators where standard echoes of similar nature (filamentation of phase space) have been reported (see Refs. [12–15]). Fractional echoes may also find applications in the related problem of echo-enabled harmonic generation in free-electron lasers (EEHG FEL) in which highly efficient generation of short-wavelength radiation is achieved via laser manipulations over the phase space of relativistic electron beams [16–19].

This work was supported by the Conseil Régional de Bourgogne (PARI program), the CNRS, the Labex ACTION program (contract ANR-11-LABX-01-01), and the French National Research Agency (ANR) through the CoConicS program (Contract No. ANR-13-BS08-0013). We also acknowledge financial support by the Israel Science Foundation (Grant No. 746/15), and the Minerva Foundation. I.A. acknowledges support as the Patricia Elman Bildner Professorial Chair. This research was made possible in part by the historic generosity of the Harold Perlman Family.

[1] E. L. Hahn, Spin echoes, Phys. Rev. **80**, 580 (1950).
[2] R. M. Hill, and D. E. Kaplan, Cyclotron Resonance Echo, Phys. Rev. Lett. **14**, 1062 (1965).
[3] R. W. Gould, Echo phenomena, Phys. Lett. **19**, 477 (1965).
[4] R. W. Gould, T. M. O'Neil, and J. H. Malmberg, Plasma Wave Echo, Phys. Rev. Lett. **19**, 219 (1967).
[5] N. A. Kurnit, I. D. Abella, and S. K. Hartmann, Observation of a Photon Echo, Phys. Rev. Lett. **13**, 567 (1964).
[6] G. Morigi, E. Solano, B.-G. Englert, and H. Walther, Measuring irreversible dynamics of a quantum harmonic oscillator, Phys. Rev. A **65**, 040102 (2002).
[7] T. Meunier, S. Gleyzes, P. Maioli, A. Auffeves, G. Nogues, M. Brune, J. M. Raimond, and S. Haroche, Rabi Oscillations Revival Induced by Time Reversal: A Test of Mesoscopic Quantum Coherence, Phys. Rev. Lett. **94**, 010401 (2005).
[8] A. Bulatov, A. Kuklov, B. E. Vugmeister, and H. Rabitz, Echo in optical lattices: Stimulated revival of breathing oscillations, Phys. Rev. A **57**, 3788 (1998).
[9] F. B. J. Buchkremer, R. Dumke, H. Levsen, G. Birkl, and W. Ertmer, Wave Packet Echoes in the Motion of Trapped Atoms, Phys. Rev. Lett. **85**, 3121 (2000).
[10] M. F. Andersen, A. Kaplan, and N. Davidson, Echo Spectroscopy and Quantum Stability of Trapped Atoms, Phys. Rev. Lett. **90**, 023001 (2003).
[11] M. Herrera, T. M. Antonsen, E. Ott, and S. Fishman, Echoes and revival echoes in systems of anharmonically confined atoms, Phys. Rev. A **86**, 023613 (2012).
[12] G. V. Stupakov, Echo effect in hadron colliders, SSC Report SSCL-579, July 1992, http://www.osti.gov/scitech/servlets/purl/7237216/.
[13] G. V. Stupakov and S. Kauffmann, Echo effect in accelerators, SSC Report SSCL-587, September 1992, http://lss.fnal.gov/archive/other/ssc/sscl-587.pdf.
[14] L. K. Spentzouris, J. F. Ostiguy, and P. L. Colestock, Direct Measurement of Diffusion Rates in High Energy Synchrotrons Using Longitudinal Beam Echoes, Phys. Rev. Lett. **76**, 620 (1996).
[15] O. Bruning, T. Linnecon, F. Ruggio, W. Scandale, and E. Shaposhnikova, *Nonlinear and Collective Phenomena in Beam Physics* (AIP, New York, 1997), p. 155.
[16] G. Stupakov, Using the Beam-Echo Effect for Generation of Short-Wavelength Radiation, Phys. Rev. Lett. **102**, 074801 (2009).
[17] D. Xiang *et al.*, Demonstration of the Echo-Enabled Harmonic Generation Technique for Short-Wavelength Seeded Free Electron Lasers, Phys. Rev. Lett. **105**, 114801 (2010).
[18] Z. T. Zhao *et al.*, First lasing of an echo-enabled harmonic generation free-electron laser, Nat. Photon. **6**, 360 (2012).
[19] E. Hemsing, G. Stupakov, D. Xiang, and A. Zholents, Beam by design: Laser manipulation of electrons in modern accelerators, Rev. Mod. Phys. **86**, 897 (2014).
[20] G. Karras, E. Hertz, F. Billard, B. Lavorel, J.-M. Hartmann, O. Faucher, E. Gershnabel, Y. Prior, and I. Sh. Averbukh, Orientation and Alignment Echoes, Phys. Rev. Lett. **114**, 153601 (2015).
[21] R. W. Boyd, *Nonlinear Optics* (Academic Press, Boston, 1992).
[22] B. Friedrich and D. Herschbach, Alignment and Trapping of Molecules in Intense Laser Fields, Phys. Rev. Lett. **74**, 4623 (1995); Polarization of molecules induced by intense nonresonant laser fields, J. Phys. Chem. **99**, 15686 (1995).
[23] H. Stapelfeldt and T. Seideman, Aligning molecules with strong laser pulses, Rev. Mod. Phys. **75**, 543 (2003).
[24] Y. Ohshima and H. Hasegawa, Coherent rotational excitation by intense nonresonant laser fields, Int. Rev. Phys. Chem. **29**, 619 (2010).
[25] S. Fleischer, Y. Khodorkovsky, E. Gershnabel, Y. Prior, and I. Sh. Averbukh, Molecular alignment induced by ultrashort laser pulses and its impact on molecular motion, Isr. J. Chem. **52**, 414 (2012).
[26] M. Lemeshko, R. V. Krems, J. M. Doyle, S. Kais, Manipulation of molecules with electromagnetic fields, Mol. Phys. **111**, 1648 (2013).

[27] S. Pabst, Atomic and molecular dynamics triggered by ultrashort light pulses on the atto- to picosecond time scale, Eur. Phys. J. Spec. Topics **221**, 1 (2013).
[28] D. Lynden-Bell, Statistical mechanics of violent relaxation in stellar systems, Mon. Not. R. Astron. Soc. **136**, 101 (1967).
[29] A. J. Lichtenberg, *Phase-Space Dynamics of Particles* (Wiley, New York, 1969).
[30] J.-M. Hartmann and C. Boulet, Quantum and classical approaches for rotational relaxation and nonresonant laser alignment of linear molecules: A comparison for CO_2 gas in the nonadiabatic regime, J. Chem. Phys. **136**, 184302 (2012).
[31] See Supplemental Material at http://link.aps.org/supplemental/10.1103/PhysRevA.94.033404 for movie M1 that accompanies this paper.
[32] V. Loriot, P. Tzallas, E. P. Benis, E. Hertz, B. Lavorel, D. Charalambidis, and O. Faucher, Laser-induced field-free alignment of the OCS molecule, J. Phys. B **40**, 2503 (2007).
[33] S. Ramakrishna and T. Seideman, Information Content of High Harmonics Generated from Aligned Molecules, Phys. Rev. Lett. **99**, 113901 (2007).
[34] F. H. M. Faisal, A. Abdurrouf, K. Miyazaki, and G. Miyaji, Origin of Anomalous Spectra of Dynamic Alignments Observed in N_2 and O_2, Phys. Rev. Lett. **98**, 143001 (2007).
[35] S. Ramakrishna and T. Seideman, High-order harmonic generation as a probe of rotational dynamics, Phys. Rev. A **77**, 053411 (2008).
[36] S. Ramakrishna and T. Seideman, Rotational wave-packet imaging of molecules, Phys. Rev. A **87**, 023411 (2013).
[37] S. J. Weber, M. Oppermann, and J. P. Marangos, Role of Rotational Wave Packets in Strong Field Experiments, Phys. Rev. Lett. **111**, 263601 (2013).
[38] T. Kanai, S. Minemoto, H. Sakai, Quantum interference during high-order harmonic generation from aligned molecules, Nature (London) **435**, 470 (2005).
[39] R. M. Lock, S. Ramakrishna, X. Zhou, H. C. Kapteyn, M. M. Murnane, T. Seideman, Extracting Continuum Electron Dynamics from High Harmonic Emission from Molecules, Phys. Rev. Lett. **108**, 133901 (2012).
[40] K. Hartinger, R. A. Bartels, Modulation of third-harmonic generation conversion in the presence of a rotational wave packet, Opt. Lett. **33**, 1162 (2008).
[41] J. Houzet, E. Hertz, F. Billard, B. Lavorel, and O. Faucher, Molecular alignment allows low-order harmonic generation by circular light in a gas, Phys. Rev. A **88**, 023859 (2013).
[42] P. N. Butcher and D. Cotter, *The Elements of Nonlinear Optics* (Cambridge University Press, Cambridge, UK, 1990).
[43] J. R. Lalanne, A. Ducasse, and S. Kielich, *Laser-Molecule Interaction: Laser Physics and Molecular Nonlinear Optics* (John Wiley & Sons, New York, 1996).
[44] I. Sh. Averbukh and N. F. Perelman, Fractional revivals: Universality in the long-term evolution of quantum wave packets beyond the correspondence principle dynamics, Phys. Lett. A **139**, 449 (1989).
[45] J. A. Yeazell and C. R. Stroud, Jr., Observation of fractional revivals in the evolution of a Rydberg atomic wave packet, Phys. Rev. A **43**, 5153 (1991).